The Astronomical Journal, 128:1857–1867, 2004 October

OPTICAL PHOTOMETRY OF SN 1993J: 1995 TO 2003

Tianmeng Zhang,[1] Xiaofeng Wang,[1] Xu Zhou,[1] Weidong Li,[2] Jun Ma,[1] Zhaoji Jiang,[1] and Zongwei Li[3]

Received 2004 April 30; accepted 2004 June 23

ABSTRACT

We present the late-time optical photometry of supernova (SN) 1993J in M81 from 1995 February to 2003 January. The observations were performed in a set of intermediate-band filters that have the advantage of tracing the strength variations of some spectral features. SN 1993J was found to fade very slowly at late times, declining only by 0.05 ± 0.02 mag (100 days)$^{-1}$ in most of the filters from 2 to nearly 10 yr after discovery. Our data suggest that the circumstellar interaction provides most of the energy that powers the late-time optical emission of SN 1993J. This is manifested by several flux peaks seen in the rough spectral energy distributions constructed from the multicolor light curves. The flux peaks near 6600, 5800, and 4900 Å may correspond to the emission lines of Hα, Na I D + He I λ5876, and [O III] $\lambda\lambda$4959, 5007, respectively. The evolution of these emission lines suggest a power-law SN density model, as proposed by Chevalier & Fransson.

Key words: supernova: individual (SN 1993J) — techniques: photometric

1. INTRODUCTION

Supernova (SN) 1993J was visually discovered on 1993 March 28 UT by Spanish amateur astronomer Francisco Garcia-Diaz (Ripero et al. 1993). It occurred in the nearby galaxy M81 (NGC 3031; $d = 3.63 \pm 0.31$ Mpc; Freedman et al. 1994), reached a maximum brightness of $M_V = 10.8$ mag, and is the optically brightest SN in the northern hemisphere since SN 1954A. SN 1993J is classified as a "Type IIb" SN: its near-maximum spectra are similar to these of SNe II, which are characterized by strong hydrogen Balmer lines, and its nebular spectra are similar to these of SNe Ib/c that have weak hydrogen but strong He I lines (Filippenko et al. 1993; Swartz et al. 1993). Models of SN 1993J (Nomoto et al. 1993; Podsiadlowski et al. 1993; Woosley et al. 1994) suggest that the progenitor has lost all but a small amount of its hydrogen layers; thus, the shock-heated effective photosphere could quickly sink through the thin H layer into the deeper He layers during the initial expansion and the cooling phase. The light curve of SN 1993J was unlike either that of the plateau or the linear version of the typical SN II, showing two maxima similar to SN 1987A but with a faster evolution. Except for the initial peak, the light curve bears a strong resemblance to SN Ib/c.

Because of its brilliant brightness and peculiarity, SN 1993J has been extensively observed along the whole electromagnetic spectrum with telescopes from the ground and in orbit. Early observations of photometry and spectroscopy in the optical bands are reported by many authors (Schmidt et al. 1993; Wheeler et al. 1993; Filippenko et al. 1994; Lewis et al. 1994; Benson et al. 1994; Richmond et al. 1994; Prabhu et al. 1995). The optical photometry during the first 360 days after explosion are published by Barbon et al. (1995) and Richmond et al. (1996). The optical spectroscopy during SN 1993J's first 2500 days is presented by Matheson et al. (2000a, 2000b).

Late-time observations of SNe II have established that some SNe II halt their luminosity decline and remain optically detectable for years and even decades after an outburst. Continued observations of these old, evolved SNe can constrain the energy mechanism of the late-time optical emission and provide clues to the evolution of their progenitor systems.

In this paper we present the late-time photometric observations of SN 1993J from the years 1995 to 2003. We describe our observations and data reduction in § 2 and the multicolor light curves and spectral energy distribution (SED) in § 3. Discussions of the late-time energy mechanism of SN 1993J are presented in § 4, and the results are summarized in § 5.

2. OBSERVATIONS AND DATA REDUCTION

Photometric observations of SN 1993J at late times have been obtained with the 60/90 cm f/3 Schmidt telescope located at the Xinglong station of the National Astronomical Observatory of China (NAOC). A Ford Aerospace 2048×2048 CCD camera with a 15 μm pixel size is mounted at the Schmidt focus of the telescope. The field of view of the CCD is $58' \times 58'$, with a plate scale of $1''.67$ pixel^{-1}.

This telescope has a photometric system with 15 intermediate-band (FWHM $\approx$ 200–400 Å) filters covering a wavelength range from 3000 to 10000 Å (Fan et al. 1996; Yan et al. 2000; Zhou et al. 2003). The transmission curves of these filters are shown as the dashed curves in Figure 1. These filters, which were designed to avoid contamination from the strongest and most variable night-sky emission lines, were used to conduct a survey project among astronomers in Beijing, Arizona, Taipei, and Connecticut (BATC) (Fan et al. 1996). We adopt the spectrophotometric AB magnitude system in which the flux calibration is performed by observing four F subdwarfs: HD 19445, HD 84937, BD +26°2606, and BD +17°4708 (Oke & Gunn 1983). The transformation equations between the broad-band Johnson-Cousins *UBVRI* and our intermediate-band filters are (Zhou et al. 2003)

$$\begin{aligned} U &= b + 0.6801(a - b) - 0.8982 \pm 0.143, \\ B &= d + 0.2201(c - d) + 0.1278 \pm 0.076, \\ V &= g + 0.3292(f - h) + 0.0476 \pm 0.027, \\ R &= i + 0.1036 \pm 0.055, \\ I &= o + 0.7190(n - p) - 0.2994 \pm 0.064. \end{aligned} \quad (1)$$

[1] National Astronomical Observatories of China, Chinese Academy of Sciences, Beijing 100012, China; ztm@vega.bac.pku.edu.cn, wxf@vega.bac.pku.edu.cn.
[2] Department of Astronomy, University of California, Berkeley, CA 94720-3411.
[3] Department of Astronomy, Beijing Normal University, Beijing 100875, China.

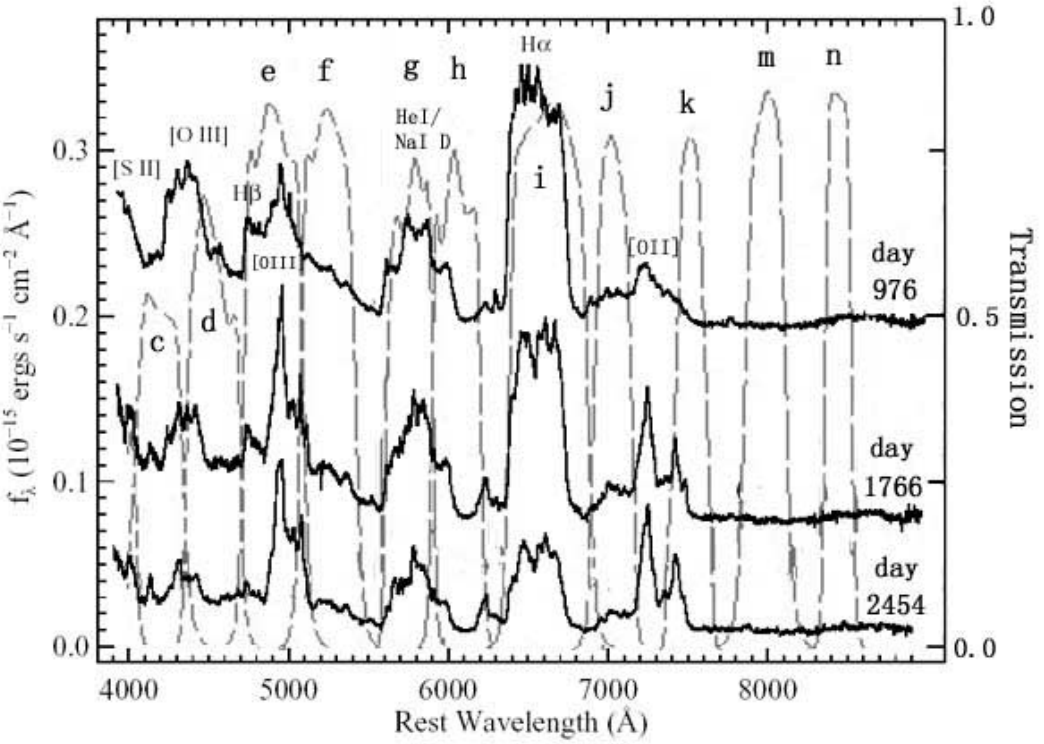

FIG. 1.—Matching of BATC intermediate-band filters with SN 1993J spectra. (The late-time spectra are taken from Matheson et al. 2000a.)

We have observed SN 1993J roughly once a year using 12 filters (*d*–*p*) since 1995. The details of the observations are given in Table 1.

2.1. *Photometry*

To obtain proper photometry of an SN that occurs in a complicated background (e.g., spiral arms or H II regions), observers are usually required to take template images of the host galaxy long after the SN has faded and do image subtraction. This method is appropriate when the SN has a relatively fast evolution and the template images can be obtained in a reasonable time. However, some SNe, as is the case for SN 1993J, are long-lived and evolve slowly during the nebular phase, and the template images cannot be obtained without the contamination of the SN light (Li et al. 2002). Therefore, we have to find an alternative method to fit the galaxy background behind SN 1993J.

TABLE 1
THE DETAILS OF BATC FILTERS AND THE OBSERVATIONS OF SN 1993J

Filter	$\lambda_{\rm eff}$ (Å)	FWHM (Å)	Limiting Magnitude	$N_{\rm obs}$[a]	$N_{\rm phot}$[b]
d.....	4540	332	20.5	6	6
e.....	4925	374	20.0	8	7
f.....	5267	344	20.0	7	4
g.....	5790	289	20.0	9	5
h.....	6074	308	20.0	5	3
i.....	6656	491	20.0	13	8
j.....	7057	238	20.0	7	7
k.....	7546	192	19.0	6	2
m.....	8023	255	19.0	4	2
n.....	8484	167	19.0	3	3
o.....	9182	247	19.0	5	3
p.....	9739	275	18.5	4	4

[a] The number of images.
[b] The number of photometric nights.

We have used a method that assumes the spiral plane around SN 1993J in M81 is a stable system that can described by a diffusive equation. This means that if the boundary condition for the equation is known, we can get the flux distribution of the spiral arm at the position of SN 1993J, and the flux of SN 1993J can be obtained by subtracting the flux of the galaxy's spiral arms from the total flux.

Before we numerically solve this Laplace equation, we do a Gaussian smoothing to reduce the noise. We then estimate the flux distribution of M81 in a circle with a 6 pixel radius centered on SN 1993J by interpolating the flux from the pixels outside the circle (see the Appendix). This process is repeated until convergence. After subtracting the estimated galaxy flux in the circle, only the flux of SN 1993J remains. Figure 2 demonstrates this process.

The final magnitudes of SN 1993J are measured on the subtracted images with standard aperture photometry. We use Pipeline II (a program developed to measure the magnitudes of point sources in BATC images), which is based on Stetson's DAOPHOT package (Stetson 1987).

2.2. *Calibration*

A total of 20 photometric nights were used to calibrate 30 local standard stars in the field of SN 1993J. For each photometric night, the aforementioned four standard stars were observed in a range of air masses, and we derive iteratively the extinction curves and the slight variation of the extinction coefficients $K+\Delta K({\rm UT})$. The instrumental magnitudes ($m_{\rm inst}$) are calibrated by the BATC AB magnitude ($m_{\rm BATC}$; Zhou et al. 2001) by

$$m_{\rm BATC} = m_{\rm inst} + [K + \Delta K({\rm UT})]\chi + C, \qquad (2)$$

where χ is the air mass, and C is the magnitude zero point.

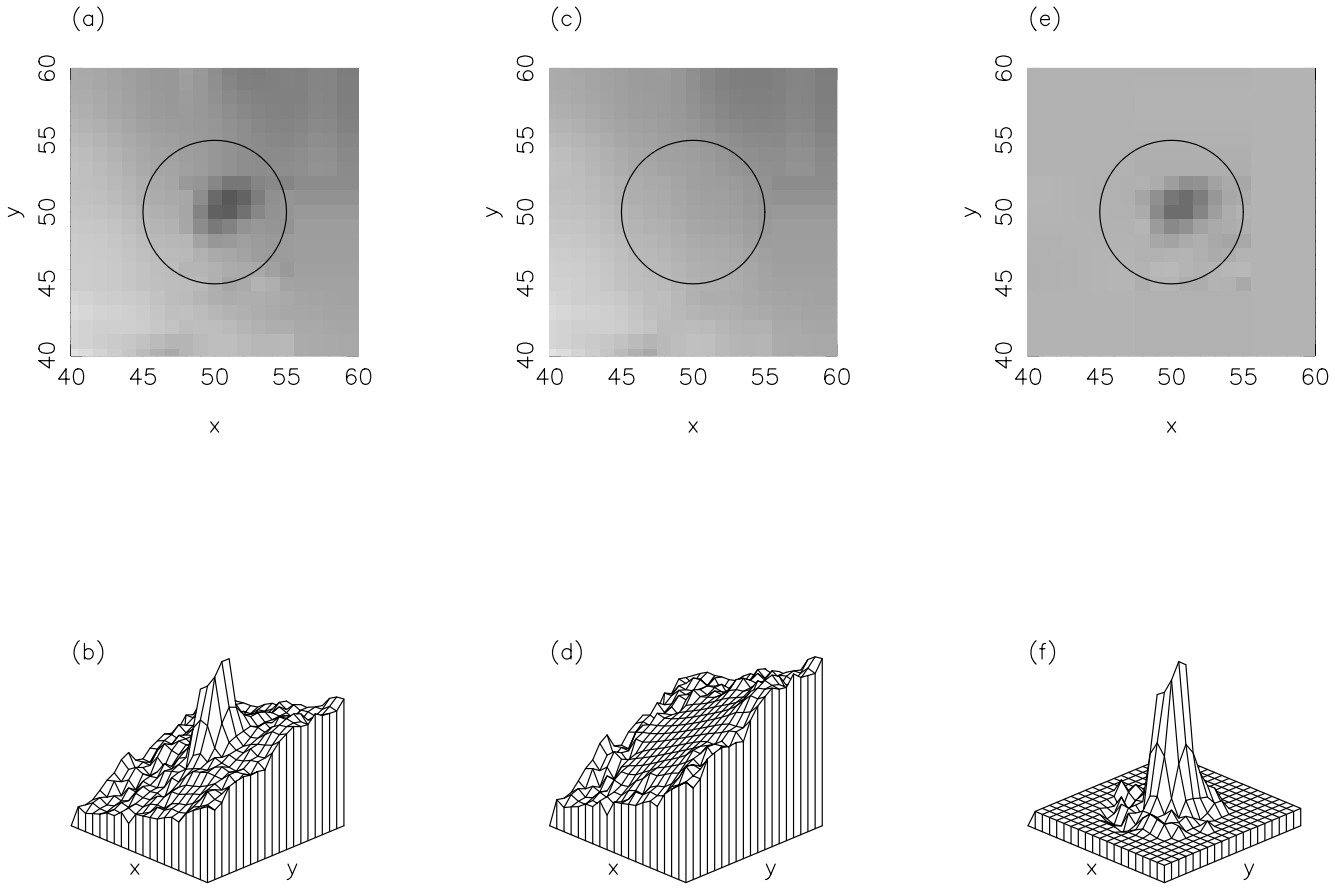

FIG. 2.—Comparison of the *i*-band image (and mesh) and the residual image (and mesh) after the fitting background subtraction. (*a*) Original image of SN1993J. (*b*) Mesh of the corresponding zone in (*a*). (*c*) Fitting background image of the SN. (*d*) Mesh of the corresponding zone in (*c*). (*e*) Image of SN 1993J after subtracting the fitting background (*d*). (*f*) Mesh of the corresponding zone in (*e*).

Table 1 lists the number of calibrations in each filter, and Table 2 lists the final calibrated BATC magnitudes and their uncertainties for the 30 local standard stars (see Fig. 3 for a parital finding chart of local standard stars). For the purpose of clearly showing the SN image, we extract a picture with a $30' \times 30'$ field of view from the original 1° image; therefore, only 5 out of 30 local standard stars are plotted in Figure 3.

These local standard stars, which are used for calibration, are listed in Table 2. The estimated error of each point is a quadrature of the uncertainties in bias and flat-field correction, aperture photometry, and calibrations (Zhou et al. 2003). The main source of the error comes from photon noise and uncertainties in the background subtraction.

We have also converted the BATC magnitudes of SN 1993J into the Johnson-Cousins system (*V*, *R*, and *I* bands), in an attempt to connect our measurements with the existing early-time broadband photometry. These converted *V*, *R*, and *I* magnitudes are listed in the last three columns in Table 3. We need to point out, however, the transformation equations we have used (also listed at the beginning of this section) are derived from observations of normal stars and could have relatively large uncertainties when applied to the emission-dominated SN 1993J during its nebular phase.

3. MULTICOLOR LIGHT CURVES

3.1. *Light Curves during the Period 1995 to 2003*

In the following sections, we adopt 1993 March 27.5 UT as the day of explosion for SN 1993J (Lewis et al. 1994). Our measured photometry of SN 1993J in the *m*, *n*, *o*, and *p* bands generally has low quality because of the low sensitivity of these filters and is discussed hereafter. The light curves of SN 1993J in other bands are shown in Figure 4*a* (*d*, *e*, *f*, and *g* bands) and Figure 4*b* (*h*, *i*, *j*, and *k* bands), respectively.

The slow luminosity decline at late times, as listed in Table 4, is evident for SN 1993J. The decline rates in various bands are generally found to be 0.05 ± 0.02 (100 days)$^{-1}$ during the years from 1995 to 2003. The light curves in the *k* and *p* bands have only a few points, so reliable decline rates cannot be determined. The slow luminosity decline of SN 1993J in all the BATC bands suggests that there is a persistent energy source powering SN 1993J up to the most recent observations.

The light curve of the *i* band, which is centered on Hα, has overall the best quality among all the bands and displays a distinct two-stage evolution: a relatively faster decline rate of 0.09 ± 0.01 mag (100 days)$^{-1}$ from 700 to 2100 days after explosion and a relatively slower decline rate of 0.02 ± 0.02 mag (100 days)$^{-1}$ from 2100 to 3600 days after explosion. The light curves in all the other bands are consistent with a linear decline at all times.

Figure 5 shows the evolution of SN 1993J in the *V*, *R*, and *I* passbands over the past decade. The earlier data are collected from Richmond et al. (1996) and Barbon et al. (1995), while those after 500 days were converted from our BATC magnitudes. All the light curves exhibit two distinct changes:, the first at about 50 days after explosion, and the second at about 400–500 days after explosion. The late-time (>500 days) decline rate of SN 1993J in *VRI* is far smaller than that between

TABLE 2

PHOTOMETRY OF COMPARISON STARS

Star	α(J2000.0)	δ(J2000.0)	d	e	f	g	h	i	j	k	m	n	o	p
1.....	09 51 20.65	68 58 09.3	13.998(04)	13.995(05)	13.779(09)	13.511(09)	13.263(08)	13.338(02)	13.267(08)	13.128(08)	13.169(05)	13.160(08)	13.013(10)	13.025(21)
2.....	09 52 10.73	69 00 10.1	15.366(10)	15.287(10)	15.065(26)	14.808(23)	14.552(23)	14.561(05)	14.476(21)	14.316(23)	14.330(12)	14.222(20)	14.209(28)	14.153(26)
3.....	09 52 55.42	69 01 01.6	14.874(07)	14.849(08)	14.646(17)	14.560(18)	14.329(19)	14.397(05)	14.328(17)	14.152(22)	14.239(10)	14.165(19)	14.116(22)	13.996(17)
4.....	09 59 31.29	69 01 57.3	14.038(04)	14.022(05)	13.811(09)	13.583(10)	13.364(08)	13.422(02)	13.424(10)	13.195(09)	13.330(06)	13.244(09)	13.166(11)	13.141(24)
5.....	09 51 37.55	69 03 52.7	15.669(13)	15.557(12)	15.364(31)	15.038(27)	14.772(26)	14.781(06)	14.797(24)	14.516(28)	14.513(13)	14.476(24)	14.321(29)	14.357(28)
6.....	10 00 30.51	69 07 47.0	16.313(20)	16.301(21)	16.030(56)	15.584(42)	15.232(24)	15.198(08)	15.043(34)	14.848(41)	14.890(19)	14.803(38)	14.714(40)	14.543(30)
7.....	09 53 16.90	69 07 02.6	15.102(08)	14.965(08)	14.831(21)	14.244(16)	13.942(13)	13.892(03)	13.770(12)	13.532(12)	13.543(06)	13.447(10)	13.354(13)	13.339(27)
8.....	09 53 41.00	69 08 06.6	14.193(05)	14.086(05)	13.895(09)	13.685(10)	13.431(09)	13.470(03)	13.421(09)	13.267(09)	13.296(05)	13.214(09)	13.177(11)	13.084(23)
9.....	09 56 44.92	69 09 00.9	15.521(11)	15.505(12)	15.267(28)	15.010(28)	14.759(26)	14.739(06)	14.706(23)	14.514(27)	14.571(14)	14.484(28)	14.406(30)	14.333(33)
10.....	09 57 15.44	69 11 29.4	16.928(34)	16.809(34)	16.605(47)	15.928(34)	15.698(31)	15.681(12)	15.564(27)	15.331(25)	15.341(27)	15.212(28)	14.948(18)	14.971(16)
11.....	09 59 20.78	69 13 19.8	15.619(12)	15.652(13)	15.449(37)	15.240(34)	15.093(37)	15.183(08)	15.102(35)	14.932(23)	15.025(22)	14.918(37)	14.797(45)	14.715(33)
12.....	09 59 03.06	69 13 53.5	16.890(33)	16.858(36)	16.651(32)	16.460(28)	15.951(27)	16.074(26)	16.076(21)	15.660(18)	15.730(28)	15.641(24)	15.519(22)	15.834(30)
13.....	09 53 27.32	69 13 53.6	14.982(08)	14.846(07)	14.712(19)	14.320(15)	13.970(14)	14.005(04)	13.947(12)	13.768(15)	13.826(08)	13.744(15)	13.637(17)	13.572(29)
14.....	09 55 14.89	69 19 26.4	14.223(05)	14.241(05)	14.102(11)	13.974(12)	13.779(13)	13.836(03)	13.814(11)	13.651(14)	13.742(07)	13.709(14)	13.641(17)	13.682(33)
15.....	09 58 12.20	69 20 11.3	14.744(07)	14.750(07)	14.624(17)	14.358(16)	14.158(15)	14.279(04)	14.309(17)	14.076(18)	14.154(10)	14.108(19)	14.050(23)	14.007(25)
16.....	09 58 35.66	69 20 47.4	14.920(08)	14.899(08)	14.789(20)	14.610(19)	14.376(20)	14.456(05)	14.413(19)	14.217(22)	14.354(11)	14.332(23)	14.157(26)	14.298(27)
17.....	09 56 16.90	69 20 43.4	15.441(11)	15.362(11)	15.132(25)	14.954(28)	14.747(28)	14.753(06)	14.700(24)	14.564(29)	14.542(13)	14.540(26)	14.457(31)	14.284(24)
18.....	09 52 54.07	69 21 15.9	14.846(07)	14.783(07)	14.660(19)	14.523(17)	14.311(18)	14.400(04)	14.354(17)	14.189(22)	14.321(10)	14.271(21)	14.134(25)	14.280(28)
19.....	09 56 18.84	69 23 43.7	15.508(12)	15.470(12)	15.344(31)	15.135(27)	14.849(29)	14.937(07)	14.818(25)	14.705(38)	14.769(17)	14.773(29)	14.783(34)	14.520(32)
20.....	09 52 21.53	69 29 30.6	15.478(12)	15.389(11)	15.317(30)	14.989(24)	14.794(28)	14.880(06)	14.783(26)	14.701(35)	14.723(16)	14.616(29)	14.628(38)	14.616(39)
21.....	09 52 09.61	69 29 56.3	17.335(46)	17.178(43)	17.083(35)	16.537(39)	16.625(37)	16.796(37)	16.493(31)	16.497(33)	16.593(34)	16.530(34)	16.219(29)	16.798(45)
22.....	09 58 47.33	69 33 14.1	15.606(12)	15.640(12)	15.499(35)	15.342(35)	15.039(34)	15.160(08)	15.099(33)	14.984(39)	14.940(18)	14.942(42)	14.957(50)	14.767(30)
23.....	09 53 49.38	69 33 56.8	15.591(13)	15.617(12)	15.366(33)	15.405(35)	15.122(39)	15.291(09)	15.236(35)	15.124(35)	15.192(26)	15.133(43)	15.023(25)	15.333(34)
24.....	09 59 56.37	69 39 19.1	14.634(06)	14.690(07)	14.495(17)	14.349(15)	14.161(17)	14.265(04)	14.246(17)	14.015(19)	14.139(10)	14.117(20)	14.072(22)	14.028(48)
25.....	09 58 21.48	69 41 17.9	15.042(08)	14.989(08)	14.789(20)	14.584(20)	14.407(21)	14.477(05)	14.492(19)	14.234(22)	14.297(11)	14.367(24)	14.218(25)	14.125(50)
26.....	10 00 03.31	69 42 44.3	16.437(24)	16.227(19)	15.894(50)	15.214(32)	14.981(31)	14.761(06)	14.632(22)	14.105(20)	14.054(09)	13.915(17)	13.796(18)	13.675(36)
27.....	09 56 49.93	69 43 51.6	17.125(41)	17.137(41)	16.736(35)	16.514(34)	16.164(37)	16.093(16)	15.933(23)	15.935(26)	15.710(34)	15.523(22)	15.456(22)	15.700(35)
28.....	09 50 16.86	69 42 54.6	16.029(17)	16.014(18)	15.900(31)	15.640(20)	15.422(25)	15.509(09)	15.486(29)	15.283(32)	15.322(28)	15.199(20)	15.269(19)	14.967(23)
29.....	09 59 21.70	69 48 37.8	15.739(13)	15.699(13)	15.504(37)	15.253(35)	15.033(35)	15.056(07)	15.017(32)	14.843(37)	14.864(17)	14.873(38)	14.752(39)	14.745(35)
30.....	09 54 34.19	69 48 36.3	15.108(09)	15.158(09)	14.927(22)	14.771(23)	14.571(24)	14.637(05)	14.604(23)	14.438(26)	14.464(13)	14.437(24)	14.438(32)	14.470(27)

NOTES.—Units of right ascension are hours, minutes, and seconds, and units of declination are degrees, arcminutes, and arcseconds. All quantities are magnitudes. Uncertainties in the last two digits are indicated in parentheses.

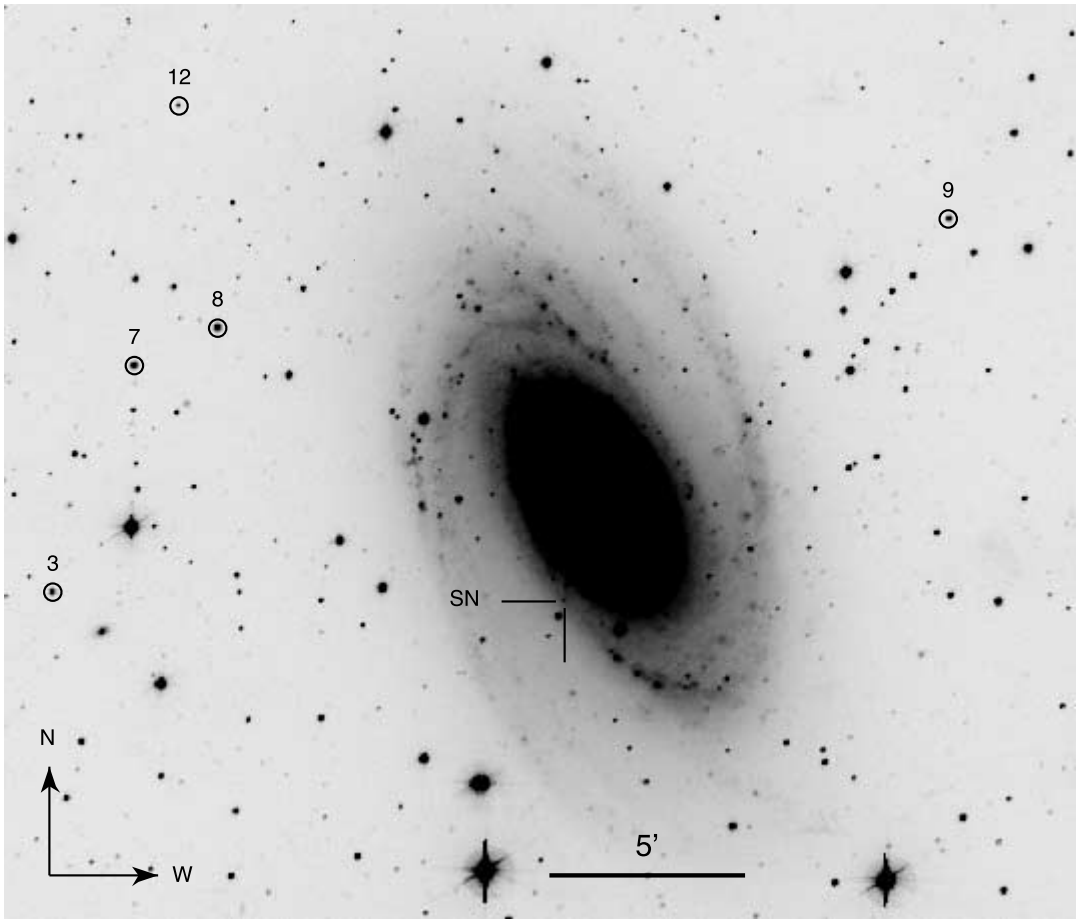

FIG. 3.—The *i*-band BATC image of the field of SN 1993J (M81), taken on 1995 December 25. The field of view is $30' \times 30'$. Five out of 30 local standard stars are marked.

50 and 360 days after explosion [0.06 ± 0.02 vs. 1.75 ± 0.03 mag (100 days)$^{-1}$]. The dramatic slowdown after 500 days could signal a change of physics for the energy source (see § 4.2 for more discussions).

We have also constructed *R*-band magnitudes from spectrophotometry based on the spectra published by Matheson et al. (2000a, 2000b), and the result is shown as filled circles in Figure 5. Their *R*-band data from spectrophotometry are generally consistent with those converted from the BATC magnitudes, except perhaps for day 881, which is nearly 2 times brighter than the neighboring points. We suspect that this might be caused by their inaccurate flux calibration.[4]

3.2. *SEDs at Several Epochs*

The late-time SED of SN 1993J can be best studied by spectroscopy, such as that done by Matheson et al. (2000a, 2000b). Alternatively, an SED could be constructed from the observed fluxes in various passbands at the same epoch. However, because of the long exposure times needed to observe SN 1993J in the intermediate bands, it is impractical to observe all bands in a single night, and our definition of the same epoch refers to a reference date plus or minus 30 days. This is reasonable, considering the very slow evolution of SN 1993J at late times.

Figure 6 shows the SEDs of SN 1993J at 700, 1000, 1423, and 3245 days after explosion. The prominent feature in the SEDs is the strong emission from the *i* band, which is an order of magnitude brighter than the neighboring *h* and *j* bands. The emissions in the *e* and *g* bands are also apparent. There is an apparent evolution in the shape of the SED: at 700 to 1000 days after explosion, the SED peaks at the *i* band, while at 3245 days after explosion, the *e* band has the strongest emission.

Figure 1 superposes the transmission curves of the BATC system on the spectral sequence of SN 1993J from Matheson et al. (2000a), and it can be seen that our intermediate-band filters have the advantage of properly covering some of the flat-topped lines of SN 1993J. Because of M81's small heliocentric velocity (-34 km s^{-1}), the *e* filter covers the emission lines near 4900 Å ([O III] $\lambda\lambda$4959, 5007 and Hβ), the *g* filter covers emission lines of He I λ5876 and Na I $\lambda\lambda$5890, 5896, and the *i* filter covers the strong Hα emission. Thus, each of the flux peaks seen in the SEDs corresponds to one or more strong emission lines in the spectra.

4. DISCUSSION

4.1. *The Late-Time Emission Lines*

We can gain some knowledge about the evolution of some emission lines from our multicolor intermediate-band light curves. In theory, measuring the emission-line intensity directly from the photometry is difficult when there is no companion knowledge of the evolution of the line profile. This problem is somewhat mitigated because our photometric passbands are intermediate in size and the transmission curves are essentially flat in each band. Moreover, the late-time spectral sequence

[4] The late-time spectra published by Matheson et al. (2000a, 2000b) did not have absolute flux calibrations.

TABLE 3

BATC 60/90 cm Schmidt Observations of SN 1993JJ

Date[a]	*d*	*e*	*f*	*g*	*h*	*i*	*j*	*k*	*m*	*n*	*o*	*p*	*V*	*R*	*I*
692.....	...	...	18.66(15)	18.24(23)	18.87(16)	17.69(05)	...	18.87(30)	...	...	...	...	18.25	17.79	...
708.....	...	18.28(11)	...	...	...	17.71(08)	18.72(26)	19.10(44)	19.16(46)	...	19.03(54)	19.19(68)	...	17.81	...
757.....	...	...	18.88(20)	18.42(10)	19.22(32)	...	...	...	...	...	...	...	18.36	...	...
982.....	...	18.47(18)	...	18.39(08)	...	...	...	...	...	...	...	...	...	...	...
1000.....	...	18.56(19)	18.96(09)	...	...	17.91(04)	...	19.11(15)	...	19.14(37)	...	...	...	18.01	...
1016.....	...	...	...	...	...	18.05(11)	18.82(29)	...	...	...	...	...	...	18.15	...
1050.....	...	...	...	...	...	17.78(05)	...	...	...	19.19(48)	19.17(43)	19.28(52)	...	17.88	18.80
1105.....	...	...	...	18.49(07)	...	...	...	19.21(58)	19.44(37)	...	18.85(60)	18.95(57)	...	...	...
1306.....	...	...	19.35(38)	19.20(61)	...	18.15(15)	...	...	...	...	...	...	...	18.25	...
1358.....	18.84(22)	...	...	...	...	18.50(18)	...	...	...	...	...	...	...	18.60	...
1423.....	18.99(41)	...	19.08(46)	18.81(30)	19.09(64)	18.38(21)	...	19.43(54)	...	...	...	...	18.85	18.48	...
1721.....	...	...	19.19(10)	18.64(46)	19.50(83)	...	19.43(99)	...	...	...	...	...	18.59	...	...
1780.....	...	...	...	...	...	18.62(15)	...	...	...	...	20.14(96)	...	...	18.72	...
2059.....	...	18.83(25)	...	...	...	...	...	...	...	...	...	...	...	...	...
2126.....	19.24(31)	...	...	19.10(26)	...	19.11(20)	19.01(94)	...	...	...	...	...	...	19.21	...
2436.....	...	...	...	...	...	...	19.54(63)	...	20.11(82)	...	...	...	...	...	...
2487.....	...	18.97(35)	...	...	...	...	...	...	...	...	...	...	...	...	...
2563.....	...	19.25(41)	...	...	...	...	...	...	...	...	...	...	...	...	...
2755.....	19.38(97)	...	...	...	...	...	...	...	...	...	...	...	...	...	...
2888.....	19.59(13)	...	...	...	...	...	...	...	...	...	...	...	...	...	...
3245.....	19.72(24)	19.02(19)	19.53(14)	19.40(12)	20.05(23)	19.28(11)	19.47(68)	20.70(99)	20.36(74)	20.28(95)	20.15(110)	20.83(126)	19.28	19.38	19.46
3504.....	...	19.15(24)	...	...	...	19.44(41)	...	...	19.44(41)	...	...	...	...	19.54	...
3620.....	...	...	...	...	...	19.44(17)	20.35(100)	...	...	...	...	...	...	19.54	...

[a] Days after explosion, 1993 March 27.5 (UT).

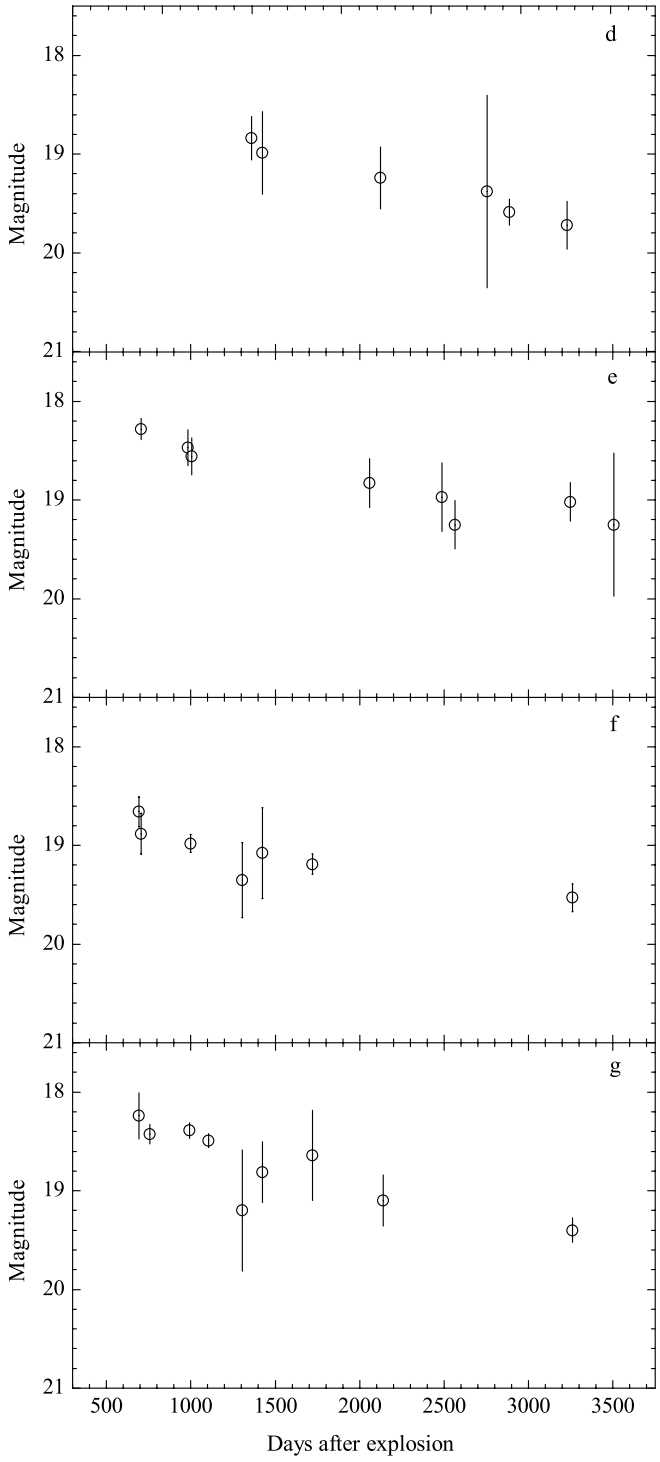

FIG. 4*a*

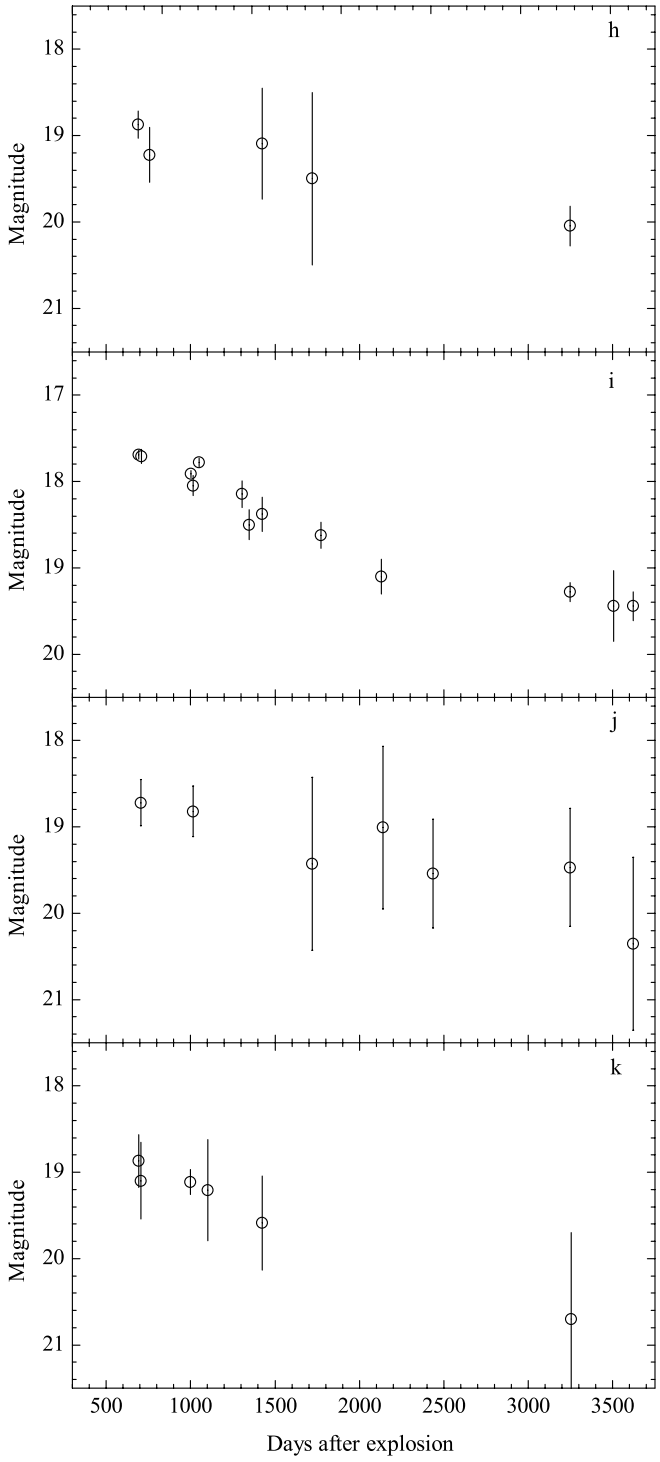

FIG. 4*b*

FIG. 4.—Light curves for SN 1993J in eight intermediate bands.

published by Matheson et al. (2000a) provides some useful information on the evolution of the line profiles. The detected emission lines in order of decreasing strength are listed below.

4.1.1. Hα *Emission*

The total line flux is calculated by summing the contributions from each unit wavelength over a range determined by the FWHM. We estimate the FWHM of the Hα line profile at different epochs from the published spectra (Matheson et al. 2000a). The FWHM of the Hα after 2500 days is unknown. According to the angular expansion revealed by Very Long Baseline Interferometry (VLBI) observations (Bartel et al. 2002), the expansion velocity of SN 1993J's radio shell does not change significantly after 1600 days. We therefore assume that the Hα line profile does not change after 2500 days. The effect of changing line width on the estimation of Hα flux will not exceed 10% even if we allow a decrease of 30 Å for the FWHM between 2500 and 3600 days.

Adopting a distance of 3.63 Mpc (Freedman et al. 1994) and $E(B-V) = 0.18$ mag toward SN 1993J (Richmond et al.

TABLE 4
LATE-TIME LUMINOSITY DECLINE RATES OF SN 1993J IN 12 INTERMEDIATE PASSBANDS

Band	Phase[a] (days)	Decline Rate (mag [100 days]$^{-1}$)
d	1358–3245	0.046 ± 0.014
e	708–3504	0.033 ± 0.007
f	692–3245	0.030 ± 0.006
g	692–3245	0.043 ± 0.006
h	692–3245	0.044 ± 0.011
i	692–3600	0.066 ± 0.004
j	708–3600	0.041 ± 0.021
k	692–3245	0.071 ± 0.037
m	708–3245	0.048 ± 0.031
n	1000–3245	0.050 ± 0.045
o	708–3245	0.054 ± 0.046
p	708–3245	0.067 ± 0.056

[a] Days after explosion, 1993 March 27.5 (UT).

1994), we estimated the reddening-corrected Hα luminosity from the *i*-band light curve. Figure 7 shows the results of our calculations. Note that the calculation does not consider the contribution by the continuum. As a result, all measurements suffer from relatively large uncertainties. We estimate the uncertainty could be as large as 30% if we consider the fluxes measured in the *m*–*p* bands as the continuum.

The current Hα emission corresponds to a luminosity of 4.0×10^{37} ergs s^{-1}. In particular, the evolution of the Hα emission from SN 1993J bears a strong resemblance to that of SN 1980K (Fesen et al. 1995). The implication of a strong persistent Hα emission at late times for SN 1993J is discussed in § 4.2.

4.1.2. He I λ5876/Na I $\lambda\lambda$5890, 5896 Emissions

The *g*-band light curve traces the emission lines of He I λ5876 and/or Na I $\lambda\lambda$5890, 5896. The luminosity of the blended lines fades very slowly from 1995 to 2002, decreasing by only ~1.2 mag. The total flux measured at the last observation (2002 March 3 UT) is 1.8×10^{-14} ergs cm^{-2} s^{-1}, which corresponds to a luminosity of 4.6×10^{37} ergs s^{-1}. Detailed

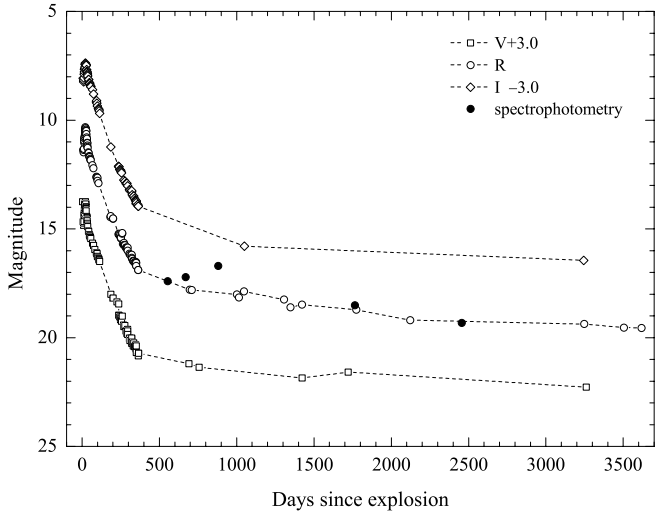

FIG. 5.—The *VRI* light curves of SN 1993J over 10 yr. An offset has been added to *V* and *I* data for clarity. The *R*-band magnitudes measured in the late-time spectra (*filled circles*) are superposed (Matheson et al. 2000a).

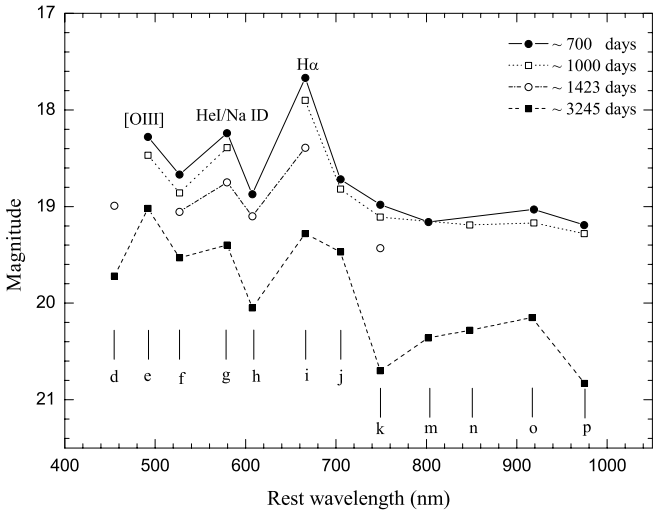

FIG. 6.—SEDs of SN 1993J at 700, 1000, 1423, and 3245 days after explosion.

analysis of the spectrum on day 976 shows that He I λ5876 and Na I $\lambda\lambda$5890, 5896 contribute approximately equally to the broad emission feature around 5800 Å (Matheson et al. 2000a). Assuming the two components have relatively the same intensity at all times, the above luminosity suggests that 8.9 yr after the SN outburst, the emission-line intensity of He I λ5876 or Na I D is about half that of the Hα.

4.1.3. [O III] $\lambda\lambda$4959, 5007 and Hβ Emissions

The *e*-band light curve traces the evolution of [O III] $\lambda\lambda$4959, 5007 and Hβ. Matheson et al. (2000a) suggested that the contribution of Hβ to the total flux peak near 4900 Å may be as high as 30%–40% before day 976 (e.g., about 40% at day 670) and decreased significantly in the following several years (e.g., 22% at day 1766 and 9% at day 2454). As a result, the late-time *e*-band light curve measures primarily the emission from the [O III] $\lambda\lambda$4959, 5007 doublets. At an earlier stage, i.e., 2–3 yr after explosion, the [O III] line emission is much weaker than Hα and the He I λ5876 + Na I D blends. At the later stage, i.e., 8–9 yr after explosion, however, the [O III] emission seems

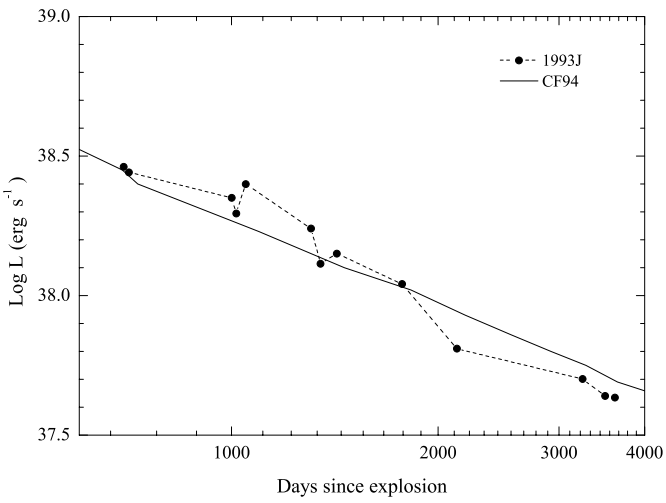

FIG. 7.—The *i*-band light curve showing the development of the Hα luminosity. Plotted are the Hα luminosity for SN 1993J over the period 1995–2003 (*filled circles*) and the predicted Hα light curve (*solid line*) from the power-law SN density model of CF94.

TABLE 5
OBSERVED LINE FLUX FROM SN 1993J

EMISSION LINE	AGE (yr)					
	1.9	2.7	4.8	5.7	8.9	9.6
Hα[a]	2.84	2.10	1.03	0.63	0.45	0.41
Na I D + He I λ5876	0.60	0.71	0.86	1.12	1.06	...
[O III] λλ4959, 5007 + Hβ	0.58	0.69	...	1.50	1.69	1.72

[a] The luminosity of Hα is in 10^{38} ergs s^{-1}.

to gain predominance over the other emission lines so that it is the strongest after 8.9 yr. The latest *e*-band measurement (2002 March 3 UT) indicates an [O III] λλ4959, 5007 luminosity of 5.7×10^{37} ergs s^{-1}, which is higher than the Hα emission at the same epoch. This is also consistent with the spectral evolution reported by Matheson et al. (2000a).

4.2. *The Energy Sources for the Late-Time Optical Emissions*

Few SNe have had optical observations up to an age of 10 yr after explosion. The late-time photometry, especially through more than one filter, provides useful information on the underlying physics for the lingering light, such as the radioactive decay of long-lived isotopes, interaction with the circumstellar medium (CSM), light echoes, and delayed optical input by finite recombination time. The question is how significant each component is.

A slow late-time decline of Hα luminosity is in agreement with the predicted energy input from ^{44}Ti decay (Woosley et al. 1989). However, ^{44}Ti or other long-lived radioactive species (^{56}Co, ^{57}Co, and ^{22}Na) are unlikely to be important energy sources for SN 1993J's optical emission at $t \approx 10$ yr, as the amount of ^{44}Ti (half-life $\simeq 60$ yr) needed to produce the current optical emissions (i.e., *i*-band emission) is 3.1×10^{-3} $(D_{\rm M81}/3.63\ {\rm Mpc})^2$ $M_\odot$, far greater than that predicted from 13–25 $M_\odot$ models (Thielemann et al. 1996) or produced in SN 1987A (Woosley et al. 1989). Thus, the radioactive mechanism is unable to explain the bulk of the optical emission of SN 1993J at the age of 10 yr. This means that some other mechanism must dominate the ionization and excitation of hydrogen.

If the progenitors of SNe emit materials for an extended period of time prior to exploding as SNe, they should be surrounded by a dusty CSM. The light from the SN explosion will scatter off this dust and produce a light echo. Since SN 1993J exploded near a spiral arm, it is expected to illuminate the interstellar and circumstellar material in the form of light echoes. It is likely that a light echo component exists in the light curves of many Type II SNe; the question is how significant the echo component is (Roscherr & Schaefer 2000). Sugerman & Crotts (2002) revealed some light echo structures around SN 1993J by analyzing archival *Hubble Space Telescope* data. They derived an observed flux from the echoes as $\sim 4.3 \times 10^{-18}$ ergs cm^{-2} s^{-1} $Å^{-1}$ in 2001, which is only about 5.4% of the Hα flux derived from our *i*-band observations at the same time (7.9×10^{-17} ergs cm^{-2} s^{-1} $Å^{-1}$). This suggests that the light echoes cannot account for the slow decay of the late-time light curves of SN 1993J.

The recombination emission might give some contribution to the optical input of supernova at late times because of the longer recombination timescales, as Kozma & Fransson (1992) showed for SN 1987A. However, the delayed recombination should not be responsible for SN 1993J's late-time energy. Comparison of the Hα luminosity from model calculations (Kozma & Fransson 1992) and observations of SN 1993J shows that the former is far smaller than the latter, e.g., $\sim 1.5 \times 10^{37}$ versus $\sim 2.8 \times 10^{38}$ ergs s^{-1} at day 700. Moreover, nonthermal emission from a young pulsar appears an equally unlikely late-time energy source. Pulsar photoionization nebulae should produce narrow emission lines ($\approx$1000 km s^{-1}; Chevalier & Fransson 1992), in contrast to the broad emission features seen in SN 1993J's late-time spectra (Matheson et al. 2000a).

Chevalier & Fransson (1994, hereafter CF94) studied mass loss before the explosion of an SN and suggested that the interaction of the SN ejecta with the circumstellar wind could provide persistent energy to power the late-time light curves. In the models CF94 studied, cool, freely expanding SN ejecta collides with the CSM from a pre-expansion stellar wind. A forward shock propagates into the wind, while a reverse shock moves back into the ejecta. The SN ejecta have a fairly steep density gradient, leading to a slow reverse shock with emission at far-UV wavelengths (possibly in X-rays, with a different gradient). This produces emission from highly ionized species. Absorption by a shell formed at the shock boundary can yield low-ionization lines, although these can also originate in the ejecta themselves. The fact that all late-time, optically detectable SNe (e.g., SNe 1957D, 1970G, 1979C, 1980K, and 1993J) exhibit strong radio emission is consistent with the idea that the main late-time energy comes from the interaction between the expanding SN shell and the slow-moving CSM. Two different models of the density profile have been considered for the structure of the wind. One is a power law, most applicable to a relatively compact progenitor, while the other uses the density structure of a red supergiant (RSG) from stellar evolution models. They make specific predictions, including the line intensity ratios and line profiles.

Table 5 lists the observed line flux ratio (relative to Hα) and the predicted values from the CF94 model, both for the power-law wind structure and the RSG model. The measured flux ratios from our data extend from 1.9 to 9.6 yr after the explosion of SN 1993J, thus providing a comparison with several epochs of the models. The flux ratios are corrected for the reddening of $E(B-V) = 0.18$ mag.

In general, the power-law density structure model provides better fits to the observed line ratios than the RSG wind model. In particular, the decrease in Hα emission from 1.9 to 9.9 yr is well reproduced (Fig. 7, *dashed lines*). Assuming Na I D contributes to half of the intensity of the emission at 5800 Å, its observed flux matches the model prediction at 2–5 yr after explosion but falls short of the prediction at 10 yr (although by only about 50%). Part of the reason for this discrepancy could be caused by the changing ratio between Na I D and He I λ5876 at very late times. The power-law density structure model of CF94, for example, predicts the Na I D line would be twice as

TABLE 6
THE PREDICTED LINE FLUX FROM CF94 MODEL

	AGE (yr)			
EMISSION LINE	2	5	10	10 (RSG)[a]
Hα[b]	0.96	0.19	0.09	0.49
Na I D	0.38	0.61	1.00	0.17
[O III] λλ4959, 5007	0.27	1.00	2.20	3.40

[a] Red supergiant model at 10 yr.
[b] The luminosity of Hα is in 10^{38} ergs s^{-1}.

strong as He I λ5876 at late times. Allowing a relatively large contribution of Hβ to the [O III] λλ4959, 5007 + Hβ blend before day 1766 (20%–40%), the observed [O III] λλ4959, 5007 flux matches the model prediction at 2 to 5 yr after explosion. At 6.7 yr, the contribution of Hβ to the [O III] + Hβ blend is less than 10%. If we assume that all flux at 5000 Å is caused by [O III] at 10 yr, we found that the observed [O III] flux does not deviate significantly from the power-law model predictions. The RSG wind model (the last column in Table 6) generally produces much stronger lines of [O III] λλ4959, 5000 and much weaker Na I D lines than observed.

5. CONCLUSIONS

We present intermediate-band photometry of SN 1993J from 692 to 3620 days after discovery, greatly extending the coverage of its evolution in the optical bands. The intermediate-band light curves show a very slow decline after day 700, fading by 0.05 ± 0.02 mag $(100 \text{ days})^{-1}$.

We constructed the SEDs of SN 1993J from the measured flux of the multicolor light curves. The SEDs show flux peaks near 4900, 5800, and 6600 Å in order of increasing strength, which are associated with the line emissions of [O III] λλ4959, 5007, Na I D/He I λ5876, and Hα, respectively. The [O III] doublet emission gains dominance over time so that it becomes the strongest emission at day 3245.

Several emission lines seen in the SEDs of SN 1993J and their evolution provide evidence that the interaction of the ejecta with the CSM is the primary energy source for powering the late-time optical emission. We also found that the power-law density profile model of the interaction model gives quantitative agreement with the observations. In particular, the line ratio of the [O III] doublet and Na II D relative to Hα are well reproduced by the model.

In the years to come, it will still be interesting to monitor the evolution of the optical emission of SN 1993J. In particular, the strength of [O III] λλ4959, 5007 will increase continuously according to the circumstellar interaction model. Continued observations of old SNe such as SN 1993J offer us an opportunity to study the transition of evolved SNe into supernova remnants.

We are grateful to Yang Yanbin for his helpful discussions about reduction of the photometric data. Financial support for this work has been provided by the National Science Foundation of China (NSFC grant 10303002; 10173003) and the National Key Basic Research Science Foundation (NKBRSF TG199075402).

APPENDIX

THE NUMERICAL SOLUTION OF THE LAPLACE EQUATION

The Laplace equation is

$$\nabla^2 U = \frac{\partial^2 U}{\partial x^2} + \frac{\partial^2 U}{\partial y^2} = 0. \quad \text{(A1)}$$

One needs the appropriate boundary conditions to solve this equation for $U(x, y)$. To solve the equation on a digital computer, it is usual to discretize the equation and to work with a finite lattice. The finite difference version of Laplace's equation is obtained by using the well-known approximations:

$$\frac{\partial^2 U}{\partial x^2} = U_{i,j-1} - 2U_{i,j} + U_{i,j+1}, \quad \text{(A2)}$$

$$\frac{\partial^2 U}{\partial y^2} = U_{i-1,j} - 2U_{i,j} + U_{i+1,j}. \quad \text{(A3)}$$

Here we use i for a row subscript, j for a column subscript, and U for the pixel value at each node of the mesh. Adding these two equations and setting the result equal to zero yields the condition that the value at any mesh point must be equal to the average of its neighbors. This is another way of defining what is known technically as a "harmonic" function. Expressed in symbols, using four grid neighbors, this gives the equation

$$U_{i,j} = \frac{1}{4}(U_{i-1,j} + U_{i+1,j} + U_{i,j-1} + U_{i,j+1}). \quad \text{(A4)}$$

REFERENCES

Barbon, R., et al. 1995, A&AS, 110, 513
Bartel, N., et al. 2002, ApJ, 581, 404
Benson, P., et al. 1994, AJ, 107, 1453
Chevalier, R. A., & Fransson, C. 1992, ApJ, 395, 540
———. 1994, ApJ, 420, 268 (CF94)
Fan, X., et al. 1996, AJ, 112, 628
Fesen, R. A., Hurford, A. P., & Matonick, D. M. 1995, AJ, 109, 2608
Filippenko, A. V., Matheson, T., & Barth, A. J. 1994, AJ, 108, 2220
Filippenko, A. V., Matheson, T., & Ho, L. C. 1993, ApJ, 415, L103
Freedman, W. L., et al. 1994, ApJ, 427, 628
Kozma, C., & Fransson, C. 1992, ApJ, 390, 602
Lewis, J. R., et al. 1994, MNRAS, 266, L27
Li, W. D., Filippenko, A. V., Van Dyk, S. D., Hu, J., Qiu, Y., Modjaz, M., & Leonard, D. C. 2002, PASP, 114, 403
Matheson, T., Filippenko, A. V., Ho, L. C., Barth, A. J., & Leonard, D. C. 2000a, AJ, 120, 1499
Matheson, T., et al. 2000b, AJ, 120, 1487
Nomoto, K., Suzuki, T., Shigeyama, T., Kumagai, S., Yamaoka, H., & Saio, H. 1993, Nature, 364, 507
Oke, J. B., & Gunn, J. E. 1983, ApJ, 266, 713
Podsiadlowski, P., Hsu, J. J. L., Joss, P. C., & Ross, R. R. 1993, Nature, 364, 509
Prabhu, T. P., et al. 1995, A&A, 295, 403
Richmond, M. W., Treffers, R. R., Filippenko, A. V., & Paik, Y. 1996, AJ, 112, 732
Richmond, M. W., Treffers, R. R., Filippenko, A. V., Paik, Y., Leibundgut, B., Schulman, E., & Cox, C. V. 1994, AJ, 107, 1022
Ripero, J., et al. 1993, IAU Circ, 5731, 1
Roscherr, B., & Schaefer, B. E. 2000, ApJ, 532, 415

Schmidt, B. P., et al. 1993, Nature, 364, 600
Stetson, P. B. 1987, PASP, 99, 191
Sugerman, B. E. K., & Crotts, A. P. S. 2002, ApJ, 581, L97
Swartz, D. A., et al. 1993, Nature, 365, 232
Thielemann, F. K., Nomoto, K., & Hashimoto, M. A. 1996, ApJ, 460, 408
Wheeler, J. C., et al. 1993, ApJ, 417, L71
Woosley, S. E., Eastman, R. G., Weaver, T. A., & Pinto, P. A. 1994, ApJ, 429, 300
Woosley, S. E., Pinto, P. A., & Hartmann, D. 1989, ApJ, 346, 395
Yan, H., et al. 2000, PASP, 112, 691
Zhou, X., Jiang, Z., Xue, S., Wu, H., Ma, J., & Chen, J.-S. 2001, Chinese J. Astron. Astrophys., 1, 372
Zhou, X., et al. 2003, A&A, 397, 361